Applied Catalysis B: Environmental 239 (2018) 254–259

Contents lists available at ScienceDirect

Applied Catalysis B: Environmental

journal homepage: www.elsevier.com/locate/apcatb

Carbon doped hexagonal BN as a highly efficient metal-free base catalyst for Knoevenagel condensation reaction

Xingyun Li[a,*,1], Baining Lin[b,1], Haobo Li[c,1], Qiang Yu[a], Ying Ge[a], Xiao Jin[a], Xuehua Liu[a], Yonghua Zhou[b,*], Jianping Xiao[c,*]

[a] Institute of Materials for Energy and Environment, College of Materials Science and Engineering, Qingdao University, Qingdao, 266071, China
[b] College of Chemistry and Chemical Engineering, Central South University, Changsha, 410083, China
[c] Institute of Natural Sciences, Westlake Institute for Advanced Study, Westlake University, Hangzhou, 310024, China

ARTICLE INFO

Keywords:
Knoevenagel condensation reaction
BCN
Metal free
Base catalyst
Carbon doping

ABSTRACT

Development of new heterogeneous base catalysts for Knoevenagel condensation reactions is critical for practical applications. Herein, we demonstrate that carbon doped hexagonal boron nitride (BCN) exhibits a high catalytic activity for Knoevenagel condensation of benzaldehyde with malononitrile, producing benzylidene malononitrile under mild reaction conditions. An 81.9% conversion can be achieved over BCN after 15 min reaction time, which is 1.8 times with respect to hexagonal boron nitride (*h*-BN) and 27 times over C_3N_4. Moreover, the BCN catalyst could be easily separated and recycled for several runs without obvious deactivation. Experimental results, spectroscopic characterizations, combined with first-principle calculations, suggest the reaction likely follows a dissociative adsorption mechanism on the oxygen terminated BCN edge. The C atoms doping plays a vital role in promoting the desorption of the intermediates. This study can open up a new avenue for the Knoevenagel condensation reaction with metal-free catalysis.

1. Introduction

Knoevenagel condensation is one of the most important carbon-carbon bond formation reactions to manufacture α,β-unsaturated carbonyl compounds, which are pivotal intermediates for the production of pharmaceuticals, fine chemicals etc [1–4]. Traditionally, the reaction is carried out in a homogeneous system using organic compounds (amine, pyridine, urea, piperidine etc.) or alkali hydroxides (KOH, NaOH etc.) as the base catalysts [5,6]. However, the notorious product separation and catalyst recovery are problematic, resulting in this process environmentally unfriendly [7]. Attempts have been made to support the homogeneous catalyst on porous solid materials, such as carbon nanotubes [8], SBA-15 [9], zeolite [10] etc. Nevertheless, the catalyst leaching is inevitably encountered after long-term reaction, which will lead to the product contamination [11]. Therefore, environmentally benign solid base catalysts with both high catalytic activity and recyclability are still desirable [12].

Nitrogen doped carbon materials (NC) with high surface area, tunable surface and electronic properties have emerged as a promising metal-free catalyst for a variety of applications [13–19]. In the last decade, it has witnessed a booming application of NC as solid base catalyst [20–24]. The pioneer work by H. Bitter and co-workers [25] revealed that the pyridinic N doped carbon nanotubes can catalyze Knoevenagel condensation reaction with a high efficiency. Park et al. [11] reported the remarkable performance of nitrogen-containing mesoporous carbon nitride (MCN) for the Knoevenagel condensation of ethylcynoacetate with aromatic aldehydes. It is demonstrated proton abstraction from methylenic compound can be facilitated by the basic surface of carbon materials. A higher density of nitrogen species is attractive to improve catalytic activity [26]. To this end, C_3N_4 with advantage of its unique graphitic carbon nitride structure and intrinsic abundant basic sites on surface has been attracted particular interest. [27–32] Extensive efforts have been devoted to promote the performance of C_3N_4 by synthesizing deprotonated mesoporous graphitic C_3N_4 [27], dispersing C_3N_4 on SBA-15 [33], Mg doping [34,35], boron doping [36] etc. Despite the endeavor above, a more efficient catalyst is still needed to improve the Knoevenagel condensation reaction.

Hexagonal boron nitride (*h*-BN) is a graphite analogous two-dimensional (2D) compound, featured with a distinct ionized surface, making *h*-BN an up-and-coming candidate as metal-free catalyst [37–43]. For example, Hermans et al. [44] reported that *h*-BN can catalyze propane dehydrogenation reactions with oxygen-terminated

* Corresponding authors.
E-mail addresses: xingyun_2008@sina.cn (X. Li), zhouyonghua@csu.edu.cn (Y. Zhou), jxiao@wias.org.cn (J. Xiao).
[1] These authors contribute equally to this work.

https://doi.org/10.1016/j.apcatb.2018.08.021
Received 11 July 2018; Received in revised form 4 August 2018; Accepted 7 August 2018
Available online 09 August 2018
0926-3373/

BN edges. Li et al. [45] found that armchair edge of *h*-BN was also able to catalyze acetylene hydrochlorination reaction. Furthermore, carbon doping into *h*-BN could provide an effective approach to modulate the electrical band structure, as well as to bring more active defects to *h*-BN materials. [46] It was shown the *h*-BN with carbon doping can serve as a promising photo-catalyst for the H_2 and O_2 evolution from H_2O, as well as CO_2 reduction [46]. Carbon doping could also bring more oxygen functionalized edges to improve the catalytic performance in dehydrogenation of ethylbenzene [47]. And C doped *h*-BN (BCN) with high spin density and charge density was demonstrated to be an excellent catalyst for oxygen reduction reaction (ORR) in fuel cell [48].

Herein, we report, for the first time, that carbon doped *h*-BN could catalyze Knoevenagel condensation of benzaldehyde with malononitrile to produce benzylidene malononitrile with a significantly better performance than the present used C_3N_4 catalyst. Theoretical calculations have confirmed the reaction mechanism at the oxygen sites on the edge of BCN and demonstrated that carbon doping could promote this process. Thus, this work can direct a new avenue towards the development of metal free solid catalyst for the carbon-carbon bond formation reaction.

2. Experimental

2.1. Synthesis of catalyst

Dicyanamide (6 g) and boric acid (2 g) were dissolved in 250 mL of water to form a clear solution. After evaporating water by continuously stirring at 80 °C for 10 h, the obtained white solid powder was calcined in a flowing Ar atmosphere (50 mL/min) with a temperature program of heating to 550 °C at 2 °C/min, maintaining at 550 °C for 1 h, raising temperature to 900 °C and maintaining at 900 °C for 2 h. The obtained sample is named as BCN. BN sample was synthesized with the similar procedure except to replace Ar atmosphere with NH_3. As comparison, C_3N_4 sample was synthesized by calcining dicyandiamide directly at 550 °C for 4 h at a heating rate of 2 °C/min in an air atmosphere.

2.2. Catalyst characterization

Transmission electron microscope (TEM) images were obtained on a JEOL JEM-2100. X-ray diffraction (XRD) patterns were measured on a Rigaku Ultima IV X-ray diffractometer with Cu Kα radiation (λ = 0.15418). X-ray photoelectron spectroscopy (XPS) was carried out on a Thermo Fisher ESCALAB 250Xi spectrometer with Al Kα X-ray source (1486.6 eV, conducted at 10.8 mA and 15 kV). N_2 adsorption-desorption was conducted on a Quantachrome Autosorb iQ3. The specific surface area was estimated with the Brunauer-Emmett-Teller (BET) method and the pore size distribution was calculated with Non-Local Density Functional Theory (NL-DFT). CO_2 temperature programed desorption (CO_2-TPD) experiments were carried out on a Bel-Cat with thermal conductivity detector. 50 mg sample was pretreated in helium gas for 30 min at 300 °C so as to remove water and other adsorbate. Then, after cooling down to 50 °C, the sample was saturated with CO_2 for 30 min. CO_2 -TPD profile was recorded from 50 °C to 300 °C at heating rate of 5 °C /min with a flowing He (100 mL/min).

2.3. Activity tests

The catalytic activity was tested for Knoevenagel condensation of benzaldehyde with malononitrile to benzylidene malononitrile. Typically, 2.5 mmoL of benzaldehyde and 2.5 mmoL of malononitrile in 15 mL of toluene were mixed with 100 mg of catalyst. The reaction was carried out in an 80 °C oil bath under N_2 as the protection atmosphere so as to inhibit the oxidation of benzaldehyde. Aliquots of the reactant was taken by syringe and analyzed by Shimazu GC 2010-Plus equipped with a flame ionization detector and a Rtx-5 chromatographic column (0.25 mm × 30 m). The conversion of benzaldehyde is determined by the equation of $Conv(benzaldehyde) = (C_0 - C_i)/C_0 \times 100\%$, where C_0 is the initial concentration of benzaldehyde and C_i is the real time concentration of benzaldehyde. The reaction rate is calculated by the equation: $Reaction\ rate = m_{benzaldehyde}/m_{cat}/t$, where $m_{benzaldehyde}$ represents the converted amount of benzaldehyde, m_{cat} represents the catalyst dosage, and t is the reaction time.

2.4. DFT calculation

DFT calculations were performed using Vienna *ab initio* simulation packages (VASP) [49] with the projector-augmented wave (PAW) pseudopotentials [50]. All calculations were based on the same generalized gradient approximation method with the Perdew-Burke-Ernzerhof (PBE) [51] functional for the exchange-correlation term. All structures were fully relaxed with a 2 × 1 × 1 Monkhorst-Pack [52] k-point sampling. The plane wave cutoff was set to 400 eV.

The model of BN edge was simulated with a periodically repeated BN nanoribbon in rectangular supercells, with the B and N atoms on the edge saturated with hydrogen atoms. The vacuum thickness in the direction perpendicular and parallel to the ribbon plane was ~12 and ~20 Å, respectively.

E_f was calculated as: $E_f = E_{tot} - n_B\mu_B - n_N\mu_N - n_C\mu_C - n_O\mu_O - n_H\mu_H$, where E_{tot} is the total energy of BN structure with doped C atoms and bonded oxygen atoms, n_B, n_N, n_C, n_O and n_H represent the total number of B, N, C, O, H atoms, and μ_B, μ_N, μ_C, μ_O and μ_H represent their chemical potentials, respectively. μ_B and μ_N are reference to pristine BN single layer: $\mu_B + \mu_N = \mu_{BN}$. μ_C is reference to pristine graphene single layer. μ_O and μ_H are reference to H_2 and O_2: $\mu_H = 1/2\mu(H_2)$, $\mu_O = 1/2\mu(O_2)$.

For the dissociative mechanism in Fig. 4e, ΔG_1 was calculated as: $\Delta G_1 = G(*H + *A) - G(*) - G(HA)$, where G(*H + *A) is the energy of the surface with dissociated co-adsorption species from malononitrile [*H and $*CH(CN)_2$], G(*) is the energy of bare surface, G(HA) is the energy of a desorbed malononitrile molecule [$CH_2(CN)_2$]; ΔG_2 was calculated as: $\Delta G_1 = G(*) + G(HAB) - G(*H + *A) - G(B)$, where G(B) is the energy of a benzaldehyde molecule (C_6H_5CHO), G(HAB) is the energy of combined intermediate molecule [$C_6H_5(OH)CH-CH(CN)_2$].

E_b was calculated as: $E_b = E_{tot} - E_{surface} - \mu$, where E_{tot} is the total energy of the surface with adsorption species, $E_{surface}$ is the energy of bare surface, μ is the chemical potential of the adsorption species.

3. Results and discussions

3.1. Characterization of the catalysts

With dicyanamide as C, N precursor and boric acid as B precursor, BCN samples were obtained by a simple calcination procedure in Ar atmosphere at 900 °C. The product is fluffy and soft in the color of dark grey. When the calcination atmosphere was changed to NH_3, C atoms could be removed, leading to white *h*-BN samples. As comparison, C_3N_4 was prepared by calcining dicyandiamide at 550 °C in air. From XRD patterns in Fig. 1a , we can clearly detect similar peaks at 25.8° and 42.4°, corresponding to (002) and (100) planes in *h*-BN samples [53], indicating that C atoms were successfully doped in the *h*-BN lattice. While a wider peak is evidenced for BCN, suggesting that a smaller particle size and poor crystallization were achieved by carbon doping. In comparison, the typical 2θ peaks at 13.0° and 27.2° proved the formation of C_3N_4 crystalline structure (Fig. 1a). The pore structures of the catalysts were characterized by N_2 adsorption-desorption experiments. Fig. 1b shows a typical I type isotherm for both *h*-BN and BCN. The steep N_2 uptake at low pressure indicates the presence of micropores. NL-DFT pore size distribution showed that the pore size for BCN is mainly distributed at 0.5–2 nm and there is also a small portion of pores located at 2.5 nm (Fig. 1c). As listed in Table 1, the BCN sample shows a large specific surface area of 1217.0 m^2/g, higher than *h*-BN

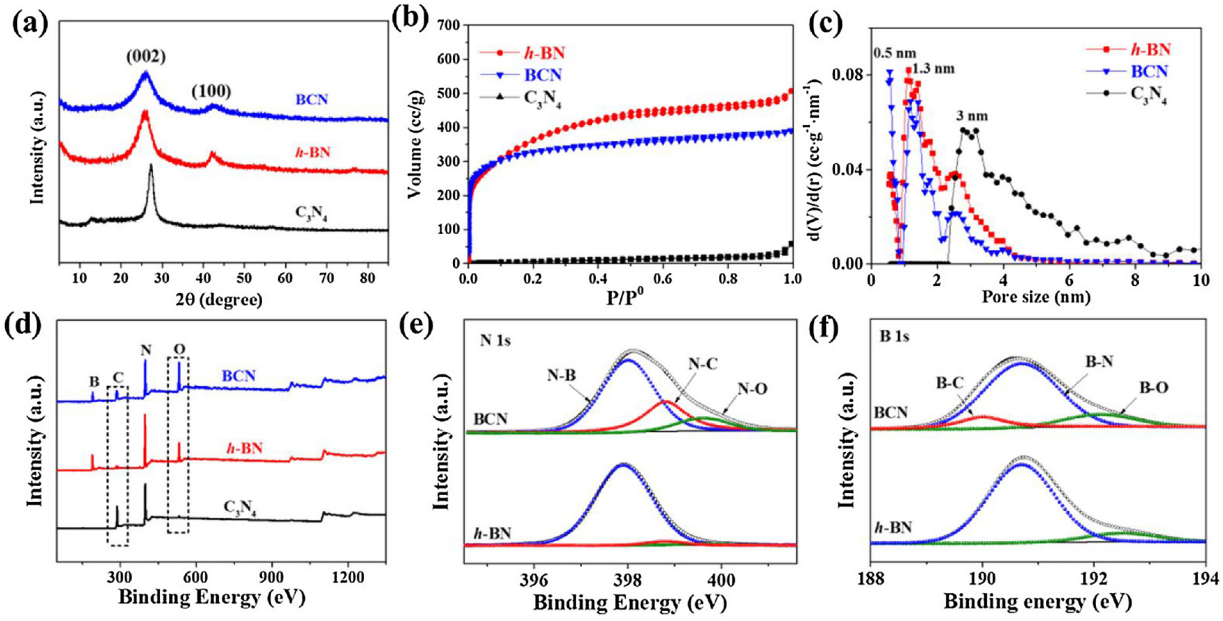

Fig. 1. (a) XRD patterns, (b) N_2 adsorption-desorption isotherms, (c) NL-DFT pore size distributions. (d) XPS spectra of BCN, *h*-BN and C_3N_4. (e) XPS N 1 s and (f) B 1 s spectrum for *h*-BN and BCN.

Table 1
pore structure and surface information of the catalysts.

	Specific surface area (m^2/g)	Pore volume (cc/g)	Average pore size (nm)	Surface composition (%)			
				B	C	N	O
BCN	1217.0	0.61	0.5 & 1.3	36.0	22.2	29.9	11.9
h-BN	1142.9	0.78	1.3	48.9	1.2	40.3	9.6
C_3N_4	29.8	0.09	3.0	0	43.5	54.9	1.6

(1142.9 m^2/g) and C_3N_4 (29.8 m^2/g). This demonstrates that carbon doping could play a great role in creation of pore structures, exposing more edges and defects for BCN samples.

XPS was used to characterize the surface composition of the catalysts. As shown in Fig. 1d, *h*-BN is mainly composed of B, N and O with negligible C. For BCN samples, we can detect the presence of C and the amount of doped C is as high as of 22.2 at. % (Table 1). Besides, there is more O element on the surface of BCN (11.9 at. %) than that of *h*-BN (9.6 at. %). Whereas, C_3N_4 is mainly composed of C and N with only 1.6 at. % of O element. From the deconvolution of N 1 s spectra shown in Fig. 1e, the binding energy at 398.0 eV can be attributed to N—B bond, while the signal at 398.8 eV corresponds to N—C and there is also abundant of N—O at 399.6 eV for BCN samples [54,55]. By fitting the B 1 s peak (Fig. 1f), it can prove the existence of B—C, B—N and B—O in BCN. From TEM image in Fig. 2a, we can see a lamella structure for BCN and EDS mapping images in Fig. 2b indicate that B, C, N, O are homogeneously distributed across the whole matrix. The HR-TEM image in Fig. 2c further reveals a stacking flake like morphology, which is similar to that of few layers graphene. The layer distance is 0.36 nm (inset in Fig. 2c), which is larger than the reported *h*-BN material (0.33 nm), indicating that C atoms doping might introduce defects and enlarge the layer space [56].

3.2. Catalytic results

The catalytic performance is evaluated for the Knoevenagel condensation of benzaldehyde with malononitrile. The blank test was first performed confirming that there is only 0.17% conversion of benzaldehyde without adding any catalyst. As shown in Fig. 3a, benzaldehyde conversion is 44.7% at reaction time of 15 min with *h*-BN as catalyst, which is much higher than that of C_3N_4. It is surprising to find that carbon doping could significantly boost the activity. An 81.9% conversion of benzaldehyde could be achieved over BCN at 15 min reaction time, which is about 1.8 times that over *h*-BN catalyst. The conversion further rises to 96% at reaction time of 1 h on BCN, corresponding to the reaction rate of 8.7 $g_{benzaldehyde} \cdot g_{cat}^{-1} \cdot h^{-1}$, ~8.5 times that of C_3N_4. The selectivity for benzylidenemalononitrile is determined to be above 99% over all the catalysts. By comparing the reaction rate with the previously reported catalyst (Table S1), we can see that BCN showed much superior activity than the CN catalyst. [57–60] This result sufficiently demonstrates that BCN is among the best solid metal-free catalysts for Knoevenagel condensation. We further verified that the

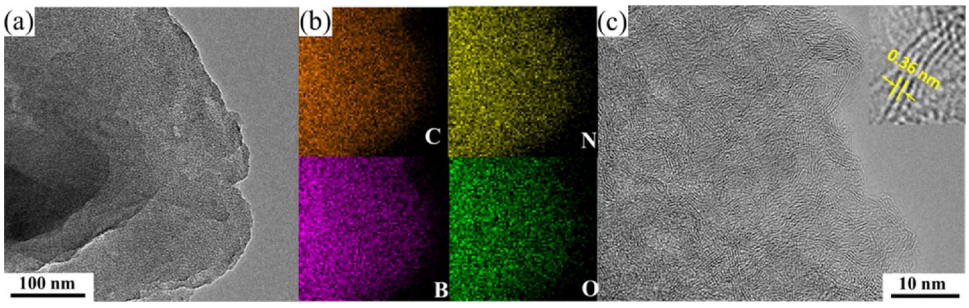

Fig. 2. (a) TEM and (b) EDS-mapping of the C, N, B, O elements. (c) HR-TEM images of BCN.

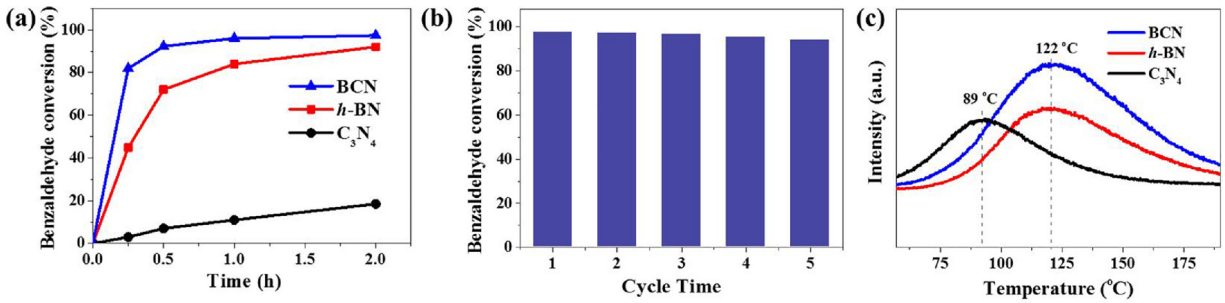

Fig. 3. (a) Conversion of benzaldehyde over BCN, *h*-BN and C_3N_4. Reaction conditions: 2.5 mmol of benzaldehyde, 2.5 mmol of malononitrile, 15 mL of toluene, 100 mg catalyst, 80 °C oil bath under N_2 as the protection atmosphere. (b) Reusability of BCN. (c) CO_2-TPD profiles of BCN, *h*-BN and C_3N_4.

catalyst remains active after 5 cycles with the conversion of 93.8% at reaction time of 2 h, validating the excellent stability of BCN (Fig. 3b). It is well documented that the basic sites on the surface make the catalysis process possible. CO_2-TPD experiments were performed to evaluate the surface basic sites. From Fig. 3c, we can see that C_3N_4 shows a CO_2 desorption temperature at 89 °C, which is about 43 °C lower than that of both *h*-BN and BCN, suggesting that both *h*-BN and BCN maintains a stronger surface basicity, while the higher CO_2 desorption peak intensity for BCN demonstrates that BCN has much higher amount of exposed basic sites with respect to *h*-BN. This result proves that carbon doping is an effective way to bring surface basicity to *h*-BN and thus improve the catalytic activity.

3.3. Reaction mechanism

In order to get a deep insight into the reaction mechanism, first-principle density functional theory (DFT) calculations have been carried out. According to the previous theoretical and experimental study, the oxygen decorated armchair edge of *h*-BN was proposed to be the active site of C–H bond activation [44]. The formation energy (E_f) of different oxygen structures on C-doped *h*-BN edge has been first calculated to evaluate the structural stability. As shown in Fig. 4a, the active oxygen structure is likely to form when the C atom substitutes the edge B atom (-0.59 eV) rather than the edge N atom (+ 0.95 eV), while it is also stable as both B and N atoms at the edge were substituted with C atoms (-0.76 eV). In the following, we name the four active sites as O_{BN}, O_{CN}, O_{BC}, and O_{CC}, respectively. As the C–O bond is pretty strong in the O_{CC} and O_{CN} systems, it makes the O—O bond broken, as shown in Fig. 4a. In other words, C atoms doped *h*-BN edge is favorable to form active oxygen sites. Such catalyst structures correspond with the XPS characterizations in Fig. 1e–f, where N—C, N—O, C—O bonds have been observed in experiments.

Moreover, the reaction mechanism on the pristine and C-doped *h*-BN edges were studied, where a malononitrile molecule (abbreviated as HA) can adsorb on the edge O site and reacts with a benzaldehyde (abbreviated as B) molecule to form a combined intermediate (HAB), forming the product of benzylidene malononitrile by producing a H_2O molecule. The activation of C—H bond of malononitrile has been considered as a crucial step [26,61]. The reaction energies of the adsorption and desorption steps are denoted as ΔG_1 and ΔG_2, respectively, where ΔG_1 indicate the formation of the adsorption intermediates. As shown in Fig. 4b, the ΔG_1 of the dissociative pathway is generally lower than the formation of corresponding isolated free radicals, which indicate that the reaction is more likely to follow the dissociative pathway on the O edge sites of catalyst surface. Thus, as shown in Fig. 4e, the reaction mechanism is proposed along a dissociative pathway, with the dissociative species (*H + *A) co-adsorbed on the two O atoms on the edge.

Based on the dissociative mechanism, we compared the activity of different structures to study the effects of doped C atoms on the activity of *h*-BN edges. According to the Sabatier principle [62], the catalytic activity is correlated with the binding energy of the intermediate on the catalyst surface, with the optimal activity achieved at an intermediate binding strength, thus the binding energies (E_b) of the dissociative co-adsorption species of malononitrile on different active site structures were calculated to compare the reactivity. ΔG_1 and ΔG_2 of the dissociative pathway (shown in Fig. 4e) were then calculated to locate the optimal reactivity, as the reaction has to go through the hardest step, that is, to overcome the highest reaction energy. As shown in Fig. 4c, generally the E_b becomes weaker along with the C atoms doping, and ΔG_1 and ΔG_2 show linear correlation with E_b, exhibiting two lines with opposite slopes for the adsorption and desorption steps, respectively. Moreover, the trend of crucial reaction energies follows the dark blue arrows, with the intersection point indicating the best activity. Among the studied four structures, the O_{CN} structure show highest activity, followed by the O_{CC} structure, while O_{BC} and O_{BN} showing lower activity. Note that O_{CN} is quite stable on the *h*-BN edge too (Fig. 4a), therefore, C atoms doping in *h*-BN edge is likely to form O_{CN} structure, which greatly promote the desorption of the reaction species on the active site in relative to O_{BN}, explaining well with the experimental observation in Fig. 3a, where BCN exhibits a significant enhanced reactivity compared to *h*-BN. Yet too much C atoms doping may not be conducive for promoting the reaction due to the formation of the O_{CC} structure. We further calculate the projected density of states (PDOS) as shown in Fig. 4d, for pristine BN (O_{BN}), the strong coupling of the electronic states from O and the reactant occur about 0.7 eV below the Fermi level, indicating that the C atoms from the reactant bind strongly on the active O sites, rationalizing well the strong adsorption of the intermediate on surfaces. While for C-doped case (O_{BC}), the coupling electronic states between C of the reactant and active O site shift upper, corresponding to the weaker interactions. For O_{CN} and O_{CC} cases, there are not obvious strong coupling of the electronic states from O and C around the Fermi level, explaining well again the role of C doping in weakening the interaction. In summary, the reaction proceeds along the dissociative adsorption mechanism. The most active site is the oxygen terminated O_{CN} structure formed on the BCN edge. As the C atom doping weakens the adsorption of intermediates on the surface, it can promote desorption of products and the overall activity.

3.4. Versatility test of the catalysts

To probe the versatility of BCN for Knoevenagel condensation reactions, a variety of aldehydes and methylene group-containing nitrides were studied and the results were summarized in Table 2. For the Knoevenagel condensation between malononitrile with aromatic aldehydes, aliphatic aldehydes, furfural, orcyclohexanone (entries 1–7), the BCN samples exhibit far better catalytic performance compared to those reported non-metal solid base catalysts in references [27,36]. This proved that BCN could serve as an efficient catalyst for reactions with different kinds of aldehydes. Nevertheless, the catalytic activity is decreased obviously when malononitrile was replaced with ethyl cyanoacetate or diethyl malonate (entries 8–9). Traditionally, this can be

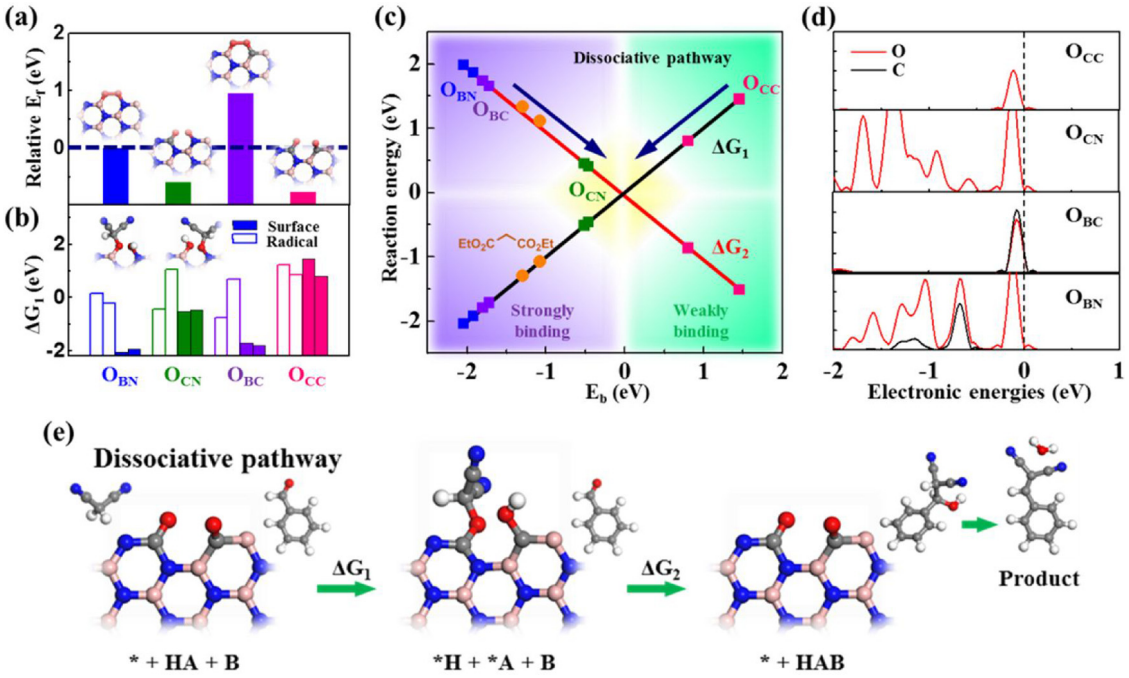

Fig. 4. (a) Formation energies (E_f) of different active sites on C-doped *h*-BN edge relative to a pristine *h*-BN edge. A lower formation energy indicates better stability. (b) Calculated reaction free energy for the formation of the intermediate (ΔG_1) on different active site structures. A lower free energy indicates a better stability. The two bars in the same color represent different adsorption configurations with asymmetric structures. Solid stripe: surface reaction; open stripe: radical formation. (c) The calculated reaction energy is linearly correlated with the binding energy (E_b) of the reaction intermediates on surface. A lower free energy indicates better favorability. A negative E_b indicates stronger reactivity. The intersection point for the adsorption (ΔG_1, black line) and the desorption (ΔG_2, red line) steps indicates the most favorable reactivity. Different active structures (blue: O_{BN}; purple: O_{BC}; green: O_{CN}; pink: O_{CC}) were indicated on the lines with two configurations each. (d) Projected density of states (PDOS) of the active O atoms (red) and the reactant C (black) binding on the active sites for the four structures O_{BN}, O_{BC}, O_{CN} and O_{CC}. The position of the Fermi level is shown in dashed lines. (e) Schematics for proposed dissociative mechanism of Knoevenagel condensation on the active sites on C-doped *h*-BN edge. HA and B represent malononitrile and benzaldehyde, respectively, with H represents the hydrogen atom. The orange dots represent diethyl malonate activation on O_{CN}. B: pink; N: blue; C: grey; O: red; H: white (For interpretation of the references to colour in this figure legend, the reader is referred to the web version of this article).

Table 2
Catalytic activity of BCN in various Knoevenagel condensation reactions.

Entry	Aldehydes	Nitriles	Conversion of benzaldehyde (%)		
			5min	15min	30min
1	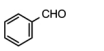		–	81.89	92.34
2[a]	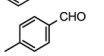		43.01	66.44	79.08
3	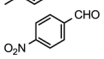		24.11	71.95	82.27
4	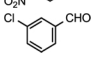		14.31	53.72	76.10
5			94.41	99.68	–
6			92.45	96.68	98.94
7			27.09	46.09	65.93
8	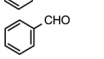		5.13	29.30	49.02
9	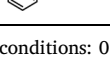		0.21	0.79	1.43

Reaction conditions: 0.1 g of catalyst, 2.5 mmol of aldehydes and 2.5 mmol of nitriles dissolved in 15 mL of methylbenzene at 80 °C.

[a] Acetonitrile was used as solvent since p-methyl benzaldehyde is not dissolved in methylbenzene.

attributed to the weaker electron-withdrawing ability of −COOEt than that of −CN, which results in the activity decrease of the H atoms in methylene compounds. Accordingly, the reaction energy of diethyl malonate on the O_{CN} site has also been calculated. As shown by the orange dots in Fig. 4c, the reaction activity of diethyl malonate is significantly lower than malononitrile, consistent well with the experiments. Moreover, the orange dots appear on the left part of the intersection, indicating the desorption step is rate-limiting.

4. Conclusions

Carbon doped *h*-BN was developed as new catalytic system for Knoevenagel condensation of benzaldehyde with malononitrile to produce benzylidenemalononitrile. The results showed that carbon doping could bring more basicity to the *h*-BN surface leading to an excellent activity and good stability. Theoretical study showed that the O site on the edge could act as the active sites and O_{CN} is most active. The reaction likely follow a dissociative adsorption mechanism, where the C—H bond break, with the proton and the rest part adsorbed on neighboring O sites. Carbon doping can promote the desorption of such intermediate structure, thereby obtaining high catalytic activity. This study could open up new possibility for the metal free catalysis of Knoevenagel condensation reaction and further broaden the potential applications of carbon doped *h*-BN material.

Acknowledgements

We acknowledge the financial support from Chinese Postdoctoral Science Foundation (2016M600519), Natural Science Foundation of Shandong Province, China (ZR2016BB03), the National Natural Science Foundation of China (21703113 and 21676303) and Taishan Scholars Advantageous and Distinctive Discipline Program of Shandong Province, China.

Appendix A. Supplementary data

Supplementary material related to this article can be found, in the online version, at doi:https://doi.org/10.1016/j.apcatb.2018.08.021.

References

[1] R.H. Vekariya, H.D. Patel, Synth. Commun. 44 (2014) 2756–2788.
[2] B. List, Angew. Chem. Int. Ed. Engl. 49 (2010) 1730–1734.
[3] J.P. Ma, Y. Pang, M. Wang, J. Xu, H. Ma, X. Nie, J. Mater. Chem. 22 (2012) 3457–3461.
[4] L.C. Player, B. Chan, P. Turner, A.F. Masters, T. Maschmeyer, Appl. Catal. B-Environ. 223 (2018) 228–233.
[5] J. Gascon, U. Aktay, M.D. Hernandez-Alonso, G.P.M. van Klink, F. Kapteijn, J. Catal. 261 (2009) 75–87.
[6] M.G. Alvarez, A.M. Frey, J.H. Bitter, A.M. Segarra, K.P. de Jong, F. Medina, Appl. Catal. B-Environ. 134 (2013) 231–237.
[7] J. Xu, K. Shen, B. Xue, Y.X. Li, J. Mol. Catal. A-Chem. 372 (2013) 105–113.
[8] G. Tuci, L. Luconi, A. Rossin, E. Berretti, H. Ba, M. Innocenti, D. Yakhvarov, S. Caporali, C. Pham-Huu, G. Giambastiani, ACS Appl. Mater. Inter. 8 (2016) 30099–30106.
[9] X.G. Wang, K.S.K. Lin, J.C.C. Chan, S.F. Cheng, J. Phys. Chem. B 109 (2005) 1763–1769.
[10] X.F. Zhang, E.S.M. Lai, R. Martin-Aranda, K.L. Yeung, Appl. Catal. A-Gen. 261 (2004) 109–118.
[11] M.B. Ansari, H.L. Jin, M.N. Parvin, S.E. Park, Catal. Today 185 (2012) 211–216.
[12] L.B. Sun, X.Q. Liu, H.C. Zhou, Chem. Soc. Rev. 44 (2015) 5092–5147.
[13] X.Y. Li, X.L. Pan, L. Yu, P.J. Ren, X. Wu, L.T. Sun, F. Jiao, X.H. Bao, Nat. Commun. 5 (2014).
[14] L.Z. Gu, L.H. Jiang, X.N. Li, J.T. Jin, J.H. Wang, G.Q. Sun, Chin. J. Catal. 37 (2016) 539–548.
[15] Z.J. Liu, J. Yu, X.Y. Li, L.X. Zhang, D. Luo, X.H. Liu, X.W. Liu, S.B. Liu, H.B. Feng, G.L. Wu, P.Z. Guo, H.L. Li, Z.H. Wang, X.S. Zhao, Carbon 127 (2018) 636–642.
[16] D. Luo, B.B. Chen, X.Y. Li, Z.J. Liu, X.W. Liu, X.H. Liu, C. Shi, X.S. Zhao, J. Mater. Chem. A Mater. Energy Sustain. 6 (2018) 7897–7902.
[17] K. Wan, G.F. Long, M.Y. Liu, L. Du, Z.X. Liang, P. Tsiakaras, Appl. Catal. B-Environ. 165 (2015) 566–571.
[18] A. Zahoor, M. Christy, Y.J. Hwang, Y.R. Lim, P. Kim, K.S. Nahm, Appl. Catal. B-Environ. 147 (2014) 633–641.
[19] X.Y. Li, P. Li, X.L. Pan, H. Ma, X.H. Bao, Appl. Catal. B-Environ. 210 (2017) 116–120.
[20] B. Sakthivel, A. Dhakshinamoorthy, J. Colloid, Interf. Sci. 485 (2017) 75–80.
[21] X. Jin, V.V. Balasubramanian, S.T. Selvan, D.P. Sawant, M.A. Chari, G.Q. Lu, A. Vinu, Angew. Chem. Int. Ed. Engl. 48 (2009) 7884–7887.
[22] K.F. Ortega, R. Arrigo, B. Frank, R. Schlogl, A. Trunschke, Chem. Mater. 28 (2016) 6826–6839.
[23] Z. Gao, C.Y. Li, G.L. Fan, L. Yang, F. Li, Appl. Catal. B-Environ. 226 (2018) 523–533.
[24] E. Quaranta, M. Carafa, F. Trani, Appl. Catal. B-Environ. 91 (2009) 380–388.
[25] S. van Dommele, K.P. de Jong, J.H. Bitter, Chem. Commun. (Camb.) (2006) 4859–4861.
[26] L.N. Zhang, H. Wang, W.Z. Shen, Z.F. Qin, J.G. Wang, W.B. Fan, J. Catal. 344 (2016) 293–302.
[27] F.Z. Su, M. Antonietti, X.C. Wang, Catal. Sci. Technol. 2 (2012) 1005–1009.
[28] J.J. Zhu, P. Xiao, H.L. Li, S.A.C. Carabineiro, ACS Appl. Mater. Inter. 6 (2014) 16449–16465.
[29] X. Liu, A.L. Jin, Y.S. Jia, J.Z. Jiang, N. Hu, X.S. Chen, RSC Adv. 5 (2015) 92033–92041.
[30] D. Masih, Y.Y. Ma, S. Rohani, Appl. Catal. B-Environ. 206 (2017) 556–588.
[31] J.J. Zhu, T.T. Diao, W.Y. Wang, X.L. Xu, X.Y. Sun, S.A.C. Carabineiro, Z. Zhao, Appl. Catal. B-Environ. 219 (2017) 92–100.
[32] J.W. Zhang, S. Gong, N. Mahmood, L. Pan, X.W. Zhang, J.J. Zou, Appl. Catal. B-Environ. 221 (2018) 9–16.
[33] J. Xu, T. Chen, J.K. Shang, K.Z. Long, Y.X. Li, Microporous Mesoporous Mater. 211 (2015) 105–112.
[34] Q.F. Deng, Q.N. Li, J. Mater. Sci. 53 (2018) 506–515.
[35] J. Xu, Y. Chen, D. Ma, J.K. Shang, Y.X. Li, Catal. Commun. 95 (2017) 72–76.
[36] J.R. Wei, W.L. Shen, C.W. Zhang, Y.H. Zhou, H.Y. Liu, Catal. Today (2018), https://doi.org/10.1016/j.cattod.2018.02.041.
[37] Q.H. Weng, X.B. Wang, X. Wang, Y. Bando, D. Golberg, Chem. Soc. Rev. 45 (2016) 3989–4012.
[38] R. Huang, B.S. Zhang, J. Wang, K.H. Wu, W. Shi, Y.J. Zhang, Y.F. Liu, A.M. Zheng, R. Schlogl, D.S. Su, Chemcatchem 9 (2017) 3293–3297.
[39] Y. Wang, L.Y. Zhao, L. Shi, J. Sheng, W.P. Zhang, X.M. Cao, P.J. Hu, A.H. Lu, Catal. Sci. Technol. 8 (2018) 2051–2055.
[40] P. Chaturbedy, M. Ahamed, M. Eswaramoorthy, ACS Omega 3 (2018) 369–374.
[41] Y.X. Fang, X.C. Wang, Angew. Chem. Int. Ed. Engl. 56 (2017) 15506–15518.
[42] M.F. Zheng, J.L. Shi, T. Yuan, X.C. Wang, Angew. Chem. Int. Ed. Engl. 57 (2018) 5487–5491.
[43] L.B. Jiang, X.Z. Yuan, G.M. Zeng, Z.B. Wu, J. Liang, X.H. Chen, L.J. Leng, H. Wang, H. Wang, Appl. Catal. B-Environ. 221 (2018) 715–725.
[44] J.T. Grant, C.A. Carrero, F. Goeltl, J. Venegas, P. Mueller, S.P. Burt, S.E. Specht, W.P. McDermott, A. Chieregato, I. Hermans, Science 354 (2016) 1570–1573.
[45] P. Li, H.B. Li, X.L. Pan, K. Tie, T.T. Cui, M.Z. Ding, X.H. Bao, ACS Catal. 7 (2017) 8572–8577.
[46] C.J. Huang, C. Chen, M.W. Zhang, L.H. Lin, X.X. Ye, S. Lin, M. Antonietti, X.C. Wang, Nat. Commun. 6 (2015).
[47] F.S. Guo, P.J. Yang, Z.M. Pan, X.N. Cao, Z.L. Xie, X.C. Wang, Angew. Chem. Int. Ed. Engl. 56 (2017) 8231–8235.
[48] S.Y. Wang, L.P. Zhang, Z.H. Xia, A. Roy, D.W. Chang, J.B. Baek, L.M. Dai, Angew. Chem. Int. Ed. Engl. 51 (2012) 4209–4212.
[49] G. Kresse, J. Furthmuller, Phys. Rev. B 54 (1996) 11169–11186.
[50] P.E. Blochl, Phys. Rev. B 50 (1994) 17953–17979.
[51] J.P. Perdew, K. Burke, M. Ernzerhof, Phys. Rev. Lett. 77 (1996) 3865–3868.
[52] H.J. Monkhorst, J.D. Pack, Phys. Rev. B 13 (1976) 5188–5192.
[53] D. Saha, G. Orkoulas, S. Yohannan, H.C. Ho, E. Cakmak, J.H. Chen, S. Ozcan, ACS Appl. Mater. Inter. 9 (2017) 14506–14517.
[54] R. Goyal, B. Sarkar, A. Bag, F. Lefebvre, S. Sameer, C. Pendem, A. Bordoloi, J. Mater. Chem. A Mater. Energy Sustain. 4 (2016) 18559–18569.
[55] S. Beniwal, J. Hooper, D.P. Miller, P.S. Costa, G. Chen, S.Y. Liu, P.A. Dowben, E.C.H. Sykes, E. Zurek, A. Enders, ACS Nano 11 (2017) 2486–2493.
[56] C.L. Tan, X.H. Cao, X.J. Wu, Q.Y. He, J. Yang, X. Zhang, J.Z. Chen, W. Zhao, S.K. Han, G.H. Nam, M. Sindoro, H. Zhang, Chem. Rev. 117 (2017) 6225–6331.
[57] H.K. Min, S.H. Cha, S.B. Hong, Chem. Commun. (Camb.) 49 (2013) 1115–1117.
[58] S.F. Amarante, M.A. Freire, D.T.S.L. Mendes, L.S. Freitas, A.L.D. Ramos, Appl. Catal. A-Gen. 548 (2017) 47–51.
[59] J. Xu, Y. Wang, J.K. Shang, D. Ma, Y.X. Li, Appl. Catal. A-Gen. 538 (2017) 221–229.
[60] S. Torii, K. Jimura, S. Hayashi, R. Kikuchi, A. Takagaki, J. Catal. 355 (2017) 176–184.
[61] N. Kan-Nari, S. Okamura, S. Fujita, J. Ozaki, M. Araib, Adv. Synth. Catal. 352 (2010) 1476–1484.
[62] P. Sabatier, Ber. Dtsch. Chem. Ges. 44 (1911) 1984–2001.